Intracellular Delivery of Proteins by Protein-Recognizing Nanoparticles

Avijit Ghosh, Mansi Sharma, and Yan Zhao*

Department of Chemistry, Iowa State University, Ames, Iowa 50011-3111, U.S.A.

ABSTRACT: Intracellular delivery of proteins can directly impact dysregulated and dysfunctional proteins and is a key step in the fast growing field of protein therapeutics. The vast majority of protein-delivery systems enter cells through endocytic pathways but endosomal escape is a difficult and inefficient process, demanding fundamentally different methods of delivery. We report ultrasmall molecularly imprinted nanoparticles that bind protein targets with high specificity through their uniquely distributed surface lysine groups. The nanoparticle–protein complexes enter cells even when energy-dependent endocytic pathways are inhibited. The micromolar binding affinities of the nanoparticle for the proteins are strong enough for the cargos to be bound during loading and transportation but weak enough to be released in cytosol, for them to interact with the desired cellular targets. The nanoparticles display low cytotoxicity to cells and can be functionalized with fluorescent labels through click chemistry for easy tracking. Both the molecular imprinting and the delivery work well for proteins with a range of molecular weights and isoelectric points, affording a convenient method to manipulate cellular functions and intracellular reactions through delivered proteins.

Keywords: protein binding, intracellular delivery, molecular imprinting, nanoparticle, protein delivery

INTRODUCTION

As workhorses of cells, proteins are involved in practically every biological process. Not surprisingly, aberrant production, function, or degradation of proteins is often associated with pathological states of a cell. Although small molecule drugs and nucleic acids may be administered to help correct protein dysregulation/dysfunction, a method receiving increasing attention is the intracellular delivery of therapeutic proteins.[1,2] Protein drugs represent one of the fastest growing therapeutics,[3] frequently dominating the list of the top-selling drugs in recent years.[4]

As large hydrophilic molecules, proteins do not cross plasma membranes spontaneously. Physical methods for intracellular protein delivery include membrane perforation and microinjection, but these invasive procedures may cause cell damage.[1] Arginine-rich cell-penetrating peptides enable various hydrophilic molecules including proteins to traverse cell membranes.[5] Their conjugation to proteins, however, could alter the latter's property or intracellular location.[6] In recent years, a wide range of materials have been investigated for intracellular delivery of proteins, including self-assembled polymer networks,[7] boronic-functionalized[8] and dendritic[9] polymers, supercharged polypeptides,[10,11] multifunctional chimaeric peptides,[12] inactivated neurotoxin,[13,14] engineered virus-like particles,[15] a bacterial contractile injection system,[16] among others.[1,17]

From a fundamental point of view, in order for a material to deliver protein cargos into cells, it first needs to bind the protein using covalent or noncovalent bonds. Covalent bonding requires chemical modification of protein, which complicates the process, requires additional purification steps, and may also change the properties of the protein. A large challenge in developing noncovalent protein-delivering materials comes from the binding itself: a strong enough binding is needed during cargo loading and translocation, while the cargo still has to be released readily once it gets inside the cell. As it stands, protein recognition by synthetic materials is an unsolved problem.[18,19] Another challenge is derived from the pathway for cell entry after protein binding and, even if internalized, whether the protein can reach cytosol, the intended destination. Most polymers and nanomaterials enter cells through endocytosis[20] and endocytic escape is widely recognized as the rate-limiting step in the intracellular delivery of therapeutics.[21]

In this work, we report a class of ultrasmall polymeric nanoparticles that bind their target proteins with high specificity to help them enter cells. The micromolar binding affinities enable the nanoparticles to carry a wide range of proteins into cells and release them readily into the cytosol. The nanoparticles display low cytotoxicity to cells, despite their positive nature. The delivery occurs in the presence of endocytosis inhibitors even when ATP is depleted in the cells. The cargos, whether enzymes or other functional proteins, retain their activities inside the cells and may be used to catalyze intended reactions and modulate cellular functions.

RESULTS AND DISCUSSION

Our ultrasmall protein-binding nanoparticles are prepared through molecular imprinting.[22-24] The technique generally involves polymerization of a mixture of functional monomers (FMs) and cross-linkers in the presence of template molecules (T). Upon imprinting, the FMs turn into binding groups around the templates in the resulting polymer network. Removal of the templates leaves behind binding sites or molecular imprints ideally complementary to the original templates in size, shape, and distribution of functional groups.

Molecular imprinting of proteins is highly challenging and the few methods reported all have shortcomings,[25] as a result of difficulties associated with the large size and complex functional groups on

the protein template, insolubility of protein in organic monomers, fragile nature of protein, lack of FMs for binding protein surface groups strongly and selectively, and difficulty in the molecular recognition in water.[26] For intracellular delivery of proteins, conventional macroporous molecularly imprinted polymers (MIPs) are unsuitable due to their macroscopic nature and insolubility.

Scheme 1 shows our method to construct protein-recognizing cationic nanoparticles for intracellular delivery. Part of the motivation for developing such materials comes from the ability of small (5–10 nm) cationic gold nanoparticles to enter cells through direct membrane penetration.[27] Molecule **1** is a cationic surfactant with a tripropargylammonium headgroup and a hydrophobic tail with a polymerizable methacrylate at the end. Its micelles are used to solubilize FM **2** and 2,2-dimethoxy-2-phenylacetophenone (DMPA) in water, while a water-soluble free radical cross-linker (N,N′-methylenebisacrylamide or MBAm) is in the aqueous solution. Addition of diazide **3** and Cu(I) cross-links the micelle on the surface by the click reaction, before the protein template is added.

It is crucial that the surfactant micelles are cross-linked before the addition of the protein template, because surfactants can denature proteins. Indeed, mixing surfactant **1** and proteins in aqueous solution frequently gives a precipitate in our hands. On the other hand, surface-cross-linked micelles (SCMs) are water-soluble covalent nanoparticles with little surface activity, as the covalently cross-linked surfactants cannot diffuse away to interact with the protein and the hydrophobic tails are tucked inside.[28] FM **2** contains a highly electrophilic trifluoromethyl ketone, known to react with primary amine *quickly and reversibly* to yield a hemiaminal.[29,30] An *ortho*-amide group can promote the reaction through an intramolecular hydrogen-bond. Two such groups have been reported to bind α amino acids with an association constant of $K_a \approx 10^7\ M^{-1}$ in acetonitrile.[31]

As shown in Scheme 1, although overall hydrophobic, FM **2** contains two polar groups that should give the molecule some solubility in water, so that it can migrate into the aqueous phase to react with the surface lysine groups on the protein template. Once some hemiaminals are formed, the protein is equipped with several hydrophobic "anchors" (i.e., the FM **2**–amine hemiaminal adducts) that prefer to re-enter the SCM. For a dynamic, uncross-linked micelle, the hydrophobic voids left upon the exit of hydrophobic guests will be quickly filled by rearrangements of the surfactants (to avoid unfavorable water/hydrophobe contact if the voids are filled with water molecules). For the SCM, rearrangements of the surfactants are constrained by the cross-links and are expected to introduce stress to the cross-linked polymer network, as the network was formed in the presence of the FMs (essentially lightly imprinted for the FMs). Refilling these voids with the original guests or similarly sized hydrophobic molecules should be energetically favorable.

Once the hemiaminal moieties enter the SCM (to form the SCM–FM–protein complex shown in Scheme 1), the hydrophobic microenvironments shield the hemiaminals from water, slowing down their hydrolysis. On the other hand, any hemiaminals in the aqueous phase are expected to undergo reversible hydrolysis and reformation in a dynamic equilibrium.[29,30] Our hypothesis is that these *fast and reversible* reactions will enable the SCM–FM–protein complex to equilibrate to a state in which several nearby FM hemiaminals are stabilized simultaneously by the SCM through hydrophobic shielding. This is an example of dynamic covalent chemistry, which allows a system constructed through reversible covalent bonds to settle to the most stable state during thermodynamic equilibration.[32-35]

The micelle-solubilized DMPA is a photo initiator. UV irradiation will cross-link the micellar core with the SCM–FM–protein complex, fixing the positions of the FMs in the cross-linked micelles and converting them into protein-binding functional groups. On the other hand, MBAm is a water-soluble radical cross-linker. With the initiating and propagating radicals confined in the cross-linked micelles, MBAm molecules can only undergo polymerization when they diffuse to the surface of the micelle. A layer of hydrogen-bond-

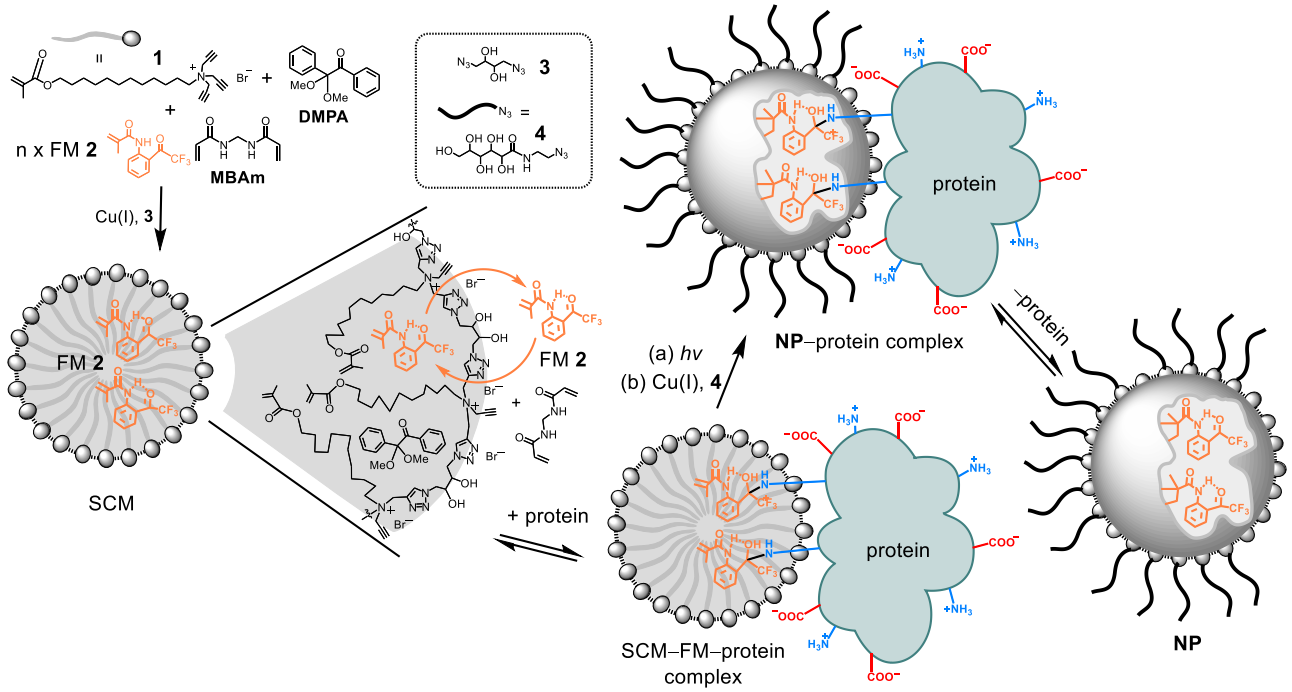

Scheme 1. Preparation of protein-recognizing nanoparticle (**NP**) via molecular imprinting of surface-cross-linked micelle (SCM). The black curved lines on the surface of the **NP** represent the clicked surface ligands **4**.

ing amide groups is expected to form near the water/surfactant interface of the micelle, with some of them fixed in the protein-binding configurations. This strategy has worked successfully in the imprinting of amphiphilic molecules such as 4-nitrophenyl-α-D-glucopyranoside, strengthening its binding by 180-fold.[36]

At the end, the doubly cross-linked nanoparticles (**NP**s) are expected to have covalently fixed trifluoromethyl ketone groups near the surface, with their number, distance, and orientation matching those of certain surface lysines on the protein (Scheme 1). The cross-linked MBAm molecules near the binding site represent secondary binding groups, supplementing the reversible covalent bonds with hydrogen bonds and help the **NPs** bind the templating protein. In addition, the binding could be strengthened by any hydrophobic/electrostatic contact established between the two binding partners. Our group has used molecularly imprinted nanoparticles to recognize proteins previously.[37] The previous method, however, relies on the imprinting of a flexible peptide sequence of the protein and thus requires both structural information of the protein and separate peptide templates. A long, flexible peptide must be present in the protein to be imprinted.

Our initial protein template for testing the design hypothesis is commercially available FITC-labelled BSA or F-BSA since its fluorescence allows its intracellular delivery to be monitored easily (*vide infra*). As shown in Table 1, **NP**(F-BSA) prepared according to Scheme 1 binds F-BSA with a binding constant (K_a) up to 49.5×10^4 M^{-1} (entry 1), as determined by isothermal titration calorimetry (ITC). The ~2 micromolar K_D value translates to nearly 7.8 kcal/mol of binding free energy ($-\Delta G$). Consistent with the design, the trifluoromethyl ketone FM **2** is critical to the binding (entries 1–4) and the binding becomes negligible in its absence, affording a relative binding constant of $K_{rel} < 0.005$ (entry 5) normalized to that of the highest binding achieved with 20 equivalents of the FM **2** (entry 1).

Table 1 shows that **NP**(F-BSA) also binds underivatized BSA, albeit with a reduced relative binding constant of $K_{rel} = 0.35$ (entry 6). This is a reasonable result because the FITC-labeling of BSA consumes some of the reactive lysine groups on the protein, and thus F-BSA differs from BSA in size, shape, and distribution of reactive lysine groups. Likewise, nanoparticles imprinted against the parent protein, i.e., **NP**(BSA), binds BSA more strongly than F-BSA (entries 7 and 8). Hence, the imprinted nanoparticles can distinguish whether the protein carries the FITC labels. The strong molecular imprinting effect is also evident from entry 9, which shows nonimprinted nanoparticles (NINPs) prepared without any templates have minimal binding for the protein. Lastly, all the nontemplating proteins tested display weak binding toward **NP**(F-BSA) (entries 10–17), highlighting the selectivity of the protein-binding nanoparticle for its target.

Among differently charged nanoparticles, cationic ones often enter cells most readily.[38-41] The zeta potential of **NP**(F-BSA), F-BSA, and an equimolar mixture of **NP**(F-BSA) and F-BSA are 26.4, -15.2, and 20.7 mV, respectively (Figure S6). Our initial experiments were indeed very promising. In the absence of the nanoparticles, minimal cell entry is observed (Figure S9a). When MDA-MB-231 cells are incubated with a 1:1 mixture of F-BSA and **NP**(F-BSA), the green fluorescent protein is clearly seen inside the cells (Figure S9b). For the samples treated with the **NP**–nanoparticle mixture, a longer incubation time leads to stronger fluorescence of the cells that seems to accumulate in the nuclei.

Table 1. ITC Binding data of **NP**(FITC-BSA)

entry	FM/Template	host	guest	K_a ($\times 10^4 M^{-1}$)	K_{rel}	$-\Delta G$ (kcal/mol)	$-\Delta H$ (kcal/mol)	$T\Delta S$ (kcal/mol)
1	20:1	**NP**(F-BSA)	F-BSA	49.5 ± 5.7	1	7.77	16.71 ± 0.64	-8.94
2	15:1	**NP**(F-BSA)	F-BSA	35.0 ± 3.6	0.70	7.56	23.79 ± 0.78	-16.23
3	10:1	**NP**(F-BSA)	F-BSA	29.3 ± 3.5	0.59	7.46	26.58 ± 1.23	-19.12
4	5:1	**NP**(F-BSA)	F-BSA	10.3 ± 1.4	0.21	6.84	3.40 ± 0.32	3.44
5	0:1	**NP**(F-BSA)	F-BSA	< 0.25 [b]	<0.005	4.64	-	-
6	20:1	**NP**(F-BSA)	BSA	17.3 ± 1.2	0.35	7.15	2.89 ± 0.08	4.26
7	20:1	**NP**(BSA)	BSA	56.5 ± 4.1	1	7.85	22.58 ± 0.64	-14.73
8	20:1	**NP**(BSA)	F-BSA	21.2 ± 1.8	0.38	7.27	1.86 ± 0.05	5.41
9	20:0	NINP	F-BSA	<0.21 [b]	<0.004	4.54	-	-
10	20:1	**NP**(F-BSA)	OVA	3.63 ± 0.62	0.073	6.22	8.42 ± 4.07	-2.19
11	20:1	**NP**(F-BSA)	HRP	4.78 ± 0.24	0.097	6.38	13.64 ± 0.77	-7.26
12	20:1	**NP**(F-BSA)	amylase	3.15 ± 0.25	0.064	6.14	17.48± 2.78	-11.34
13	20:1	**NP**(F-BSA)	lysozyme	2.22 ± 0.47	0.045	5.93	13.01 ± 4.22	-7.08
14	20:1	**NP**(F-BSA)	trypsin	< 0.87	0.018	5.38	-	-
15	20:1	**NP**(F-BSA)	transferrin	< 0.13 [b]	0.003	4.23	-	-
16	20:1	**NP**(F-BSA)	Cyt-c	2.88 ± 0.53	0.058	6.08	13.45 ± 5.40	-7.37
17	20:1	**NP**(F-BSA)	chymotrypsin	< 0.17 [b]	0.003	4.42	-	-

[a] Titrations were performed at 298K in 10 mM HEPES buffer (pH=7.5) in triplicates, with the errors among the runs <5%. **NP**(F-BSA) was prepared using a ratio of [**1**]/[**3**]/[**4**]/[MBAm]/[**2**]/[F-BSA] = 50:50:100:100:20:1. Characterization of the NPs are found in the Supporting Information (Figures S1–S6). Typical ITC titrations curves are shown in Figure S7–S8. [b] The binding constant was estimated from ITC.

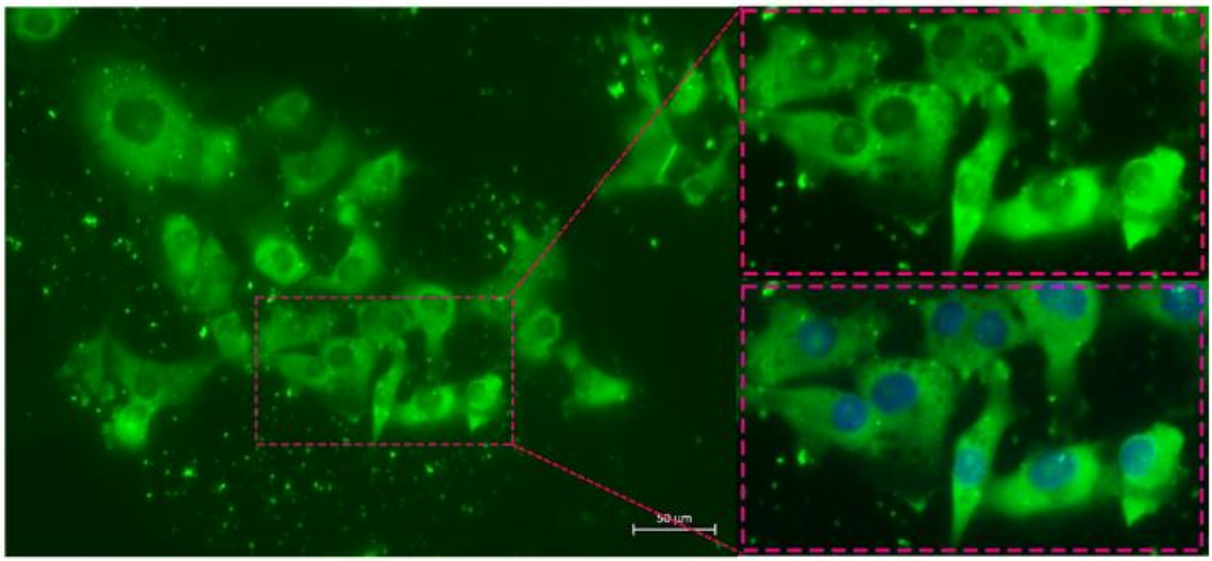

Figure 1. Fluorescent images of MDA-MB-231 cells after 2 h of incubation with 20 µM F-BSA and 20 µM of **NP**(F-BSA) at 37 °C. The nuclei were pre-stained with Hoechst 33342. The insets were magnified views of a selected region of cells, in the green channel and with overlaid green and blue channel images, respectively.

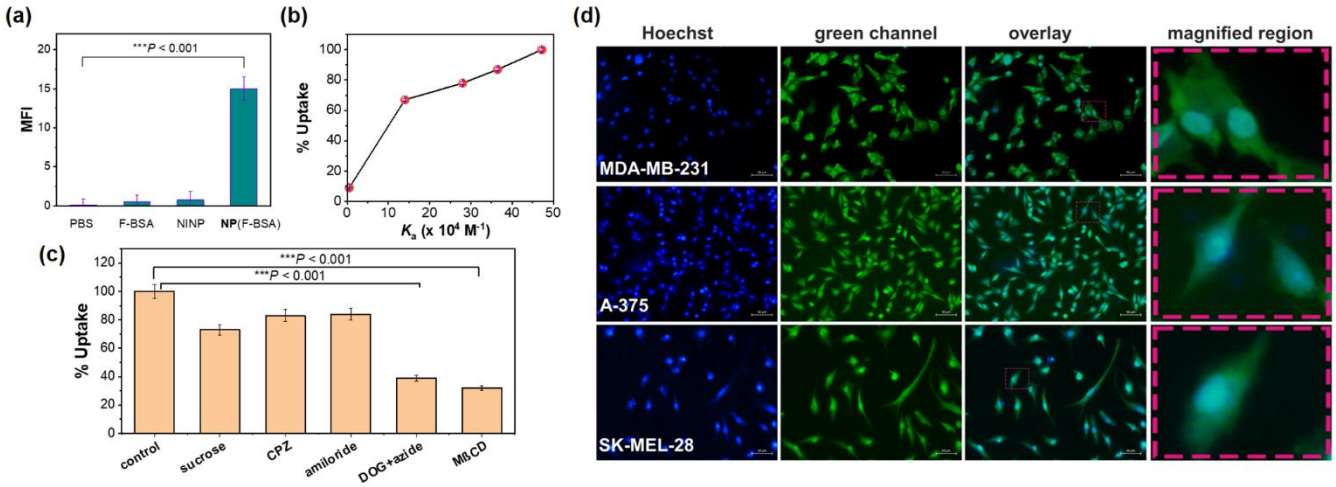

Figure 2. (a) Mean fluorescence intensity (MFI) of differently treated MDA-MB-231cells at 37 °C for 2 h: PBS buffer, 20 µM F-BSA, 20 µM F-BSA and 20 µM NINP, 20 µM F-BSA and 20 µM **NP**(F-BSA); Data are shown as mean ± SD. (n = 3). * p<0.05, ** p<0.005, *** p<0.001, ns: no significant difference. Comparison between the two groups is analyzed by independent Sample's T-test. (b) Percent uptake of F-BSA by MDA-MB-231 cells after 2 h at 37 °C as a function of the binding constant of **NP**(F-BSA) for F-BSA (Figure S10). (c) Percent uptake of F-BSA by MDA-MB-231 cells after 2 h at 37 °C in the presence of different inhibitors (Figure S11): sucrose = hypertonic sucrose; CPZ = chlorpromazine; DOG+Azide = 2-deoxy-D-glucose + sodium azide; MβCD = methyl-β-cyclodextrin; Data are shown as mean ± SD. (n = 3). * p<0.05, ** p<0.005, *** p<0.001, ns: no significant difference. Comparison between the two groups is analyzed by independent Sample's T-test. (d) Intracellular delivery of F-BSA by **NP** (F-BSA) to MDA-MB-231, A-375 and SK-MEL-28 cells after 4 h at 37 °C.

Figure 1 shows a high-resolution fluorescent image of the MDA-MB-231 cells after treatment with a 1:1 mixture of F-BSA and **NP**(F-BSA). Diffuse staining of the cells in the cytosolic region is observed while many organelles are not stained.

Figure 2a shows the normalized mean fluorescence intensity (MFI) of differently treated MDA-MB-231cells. The PBS-treated sample gives an indication for the background fluorescence which is very weak. F-BSA by itself or in the presence of NINPs also stains the cells minimally. In the presence of **NP**(F-BSA), in contrast, F-BSA is clearly able to enter cells, affording an MFI 20–30 times stronger than the value obtained with F-BSA or F-BSA + NINP. Consistent with the binding-enabled intracellular delivery, Figure 2b shows the % uptake of F-BSA by the cells correlates positively with the binding constant between the protein and **NP**(F-BSA)—the five data points in Figure 2b corresponds to the nanoparticles prepared with different amounts of FMs in Table 1 (entries 1–5).

Cell entry of nanoparticles strongly depends on their size, charge, and amphiphilicity.[20,42] Endocytosis is the dominant pathway for cationic nanoparticles 10–100 nm in size[43] but cationic gold nanoparticles <10 nm have been shown to enter cells by direct

membrane penetration.[27] Since our cross-linked micelles are ~ 5 nm in diameter and cationically charged, we reasoned there was a good chance for them to take nonendocytic pathways.

Indeed, the facilitated delivery of F-BSA by **NP**(F-BSA) is only slightly affected by two inhibitors for the clathrin-mediated endocytosis (CME), i.e., hypertonic sucrose and CPZ (chlorpromazine).[44] Thus, CME is not a major contributor (Figure 2c). Since amiloride also displays a weak inhibitory effect, micropinocytosis is not a significant pathway either.[45] 2-Deoxy-D-glucose (DOG) and sodium azide together suppress all energy-dependent cell entries by depleting ATP in the cells. Even though they inhibit the F-BSA uptake significantly, 40% of the cell uptake remains under this condition and should be derived from energy-independent pathways that remain active. Methyl-β-cyclodextrin (MβCD) depletes cholesterol from cell membranes and can inhibit CLIC/GEEC endocytosis[42] and lipid raft-mediated uptake processes such as membrane fusion and caveolae-mediated endocytosis.[46,47] Its strong inhibitory effect (Figure S9d) suggests that either these pathways are major contributors to the facilitated cell entry or the energy-independent cell entries happen in cholesterol-rich domains and/or require cholesterol to be efficient.

The intracellular delivery of F-BSA works well across different cell lines. Figure 2d shows that F-BSA with the help of **NP**(F-BSA) is able to enter MDA-MB-231, A-375, and SK-MEL-28 cells all very well and only 30–60 min of incubation period is needed to observe delivery signal from the cells (Figure S12). The nuclei of these cells are pre-stained with blue-emitting Hoechst dye before the cell uptake experiments. The fluorescence imaging indicates that the protein can enter the nuclei of all three cell types and the nuclear accumulation is particularly strong for the SK-MEL-28 cells.

Generally speaking, it is difficult for endocytosed proteins to escape endo/lysosomes,[20,21] let alone for them to enter nuclei within a short period of time. Nuclear accumulation is considered a strong indicator for cytosolic delivery, because only proteins in the cytosol can enter the nucleus (through the nuclear pore complex, as long as the protein is smaller than the 9–12 nm cutoff size).[48] Figure 2d, hence, corroborates with the above inhibitory studies (Figure 2c) and indicate that the nanoparticles could deliver proteins readily into the cytosol.

Our protein-binding nanoparticles are normally functionalized with surface ligand **4** through the click chemistry (Scheme 1). This sugar-derived monoazide is used so that the resulting nanoparticles can be precipitated from acetone while the templating protein is removed by solvent washing. To further confirm the facilitated delivery, we labeled **NP**(F-BSA) with azido-containing lissamine derivative **5** before the addition of **4**, so that the resulting **NP**(F-BSA)* can be visualized under a fluorescence microscope (Figure S13).

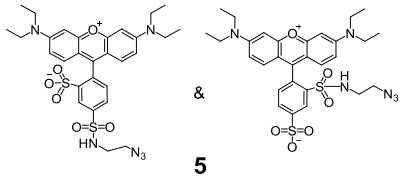

5

With F-BSA having a green emission and **NP**(F-BSA)* red, we can monitor their co-localization inside cell. For these experiments, cells were stained with the blue-emitting Hoechst nuclei dye (Figure 3a). The red channel images shows that **NP**(F-BSA)* is taken up by the cells (Figure 3b) and the green channel shows F-BSA also enters the cells (Figure 3c). Overlay of the red- and green-images shows many yellow regions (Figure 3d,e), as a result of co-localization of the protein and the nanoparticles. Some parts of the cells appear green, indicating some F-BSA proteins have been released from the nanoparticle carriers. Similar result was obtained when the experiment was carried out with other cell lines (Figure S14).

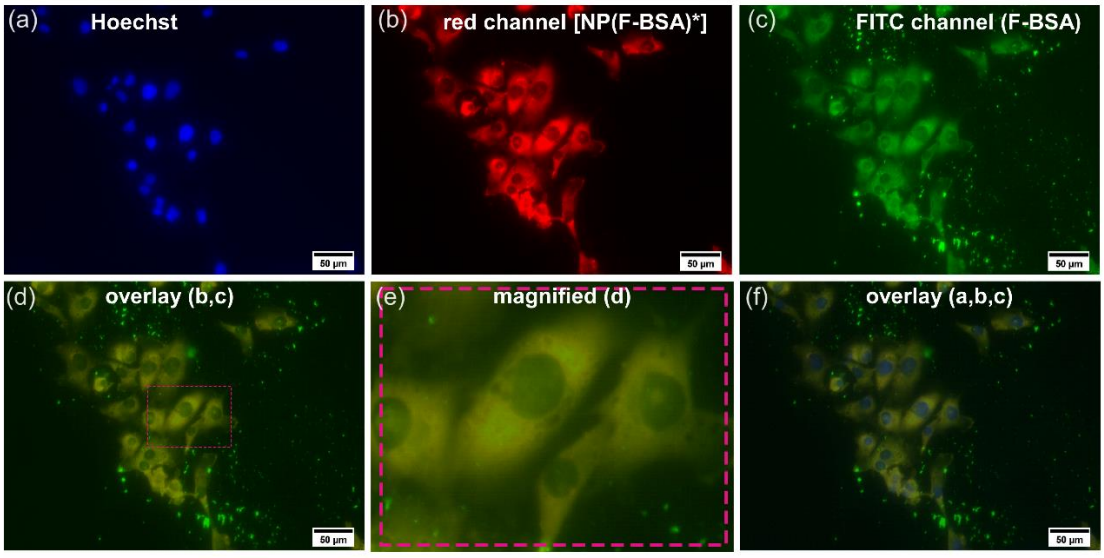

Figure 3. (a–f) Fluorescence imaging of MDA-MB-231 cells incubated with 20 μM F-BSA and **NP**(F-BSA)*: (a) image of cells in the blue channel (to visualize the nucleus-binding Hoechst 33342); (b) image of cells in the red channel (to visualize **NP**(F-BSA)*); (c) image of cells in the green channel (to visualize F-BSA); (d) overlay of the red- and the green-channel images; (e) magnified view of a selected region of cells in Figure 3d; (f) overlay of a, b and c.

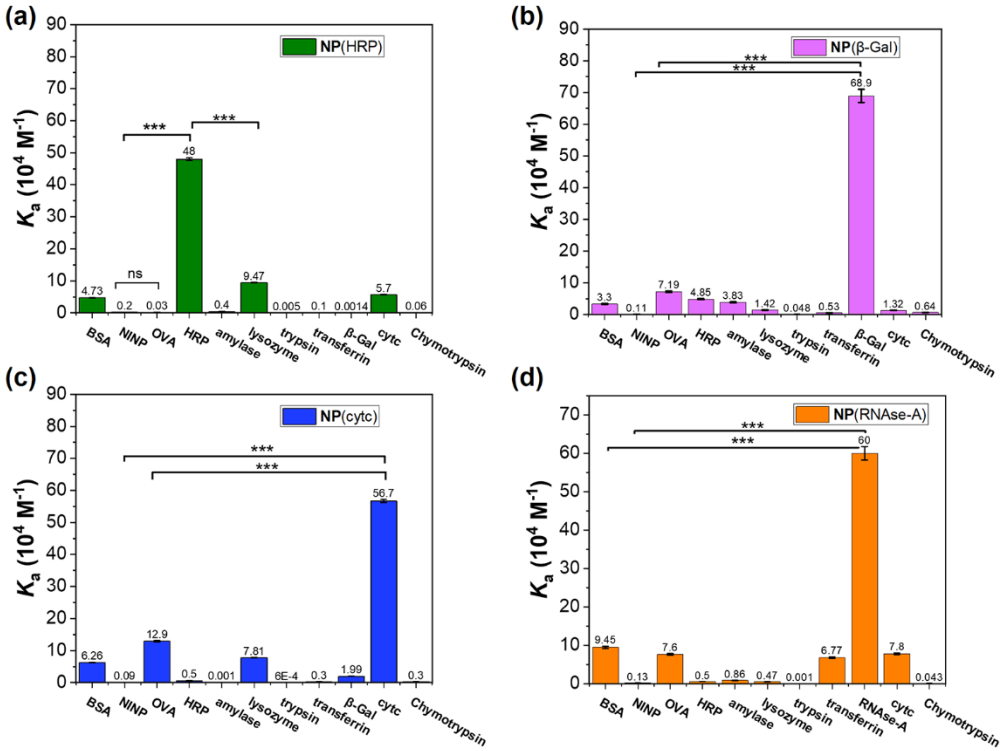

Figure 4. Binding constants of (a) **NP**(HRP), (b) **NP**(β-Gal), (c) **NP**(Cytc), and (d) **NP**(RNAse-A) for different proteins determined by ITC at 298K in 10mM HEPES buffer (pH=7.5). Data are shown as mean ± SD. (n = 3). * p<0.05, ** p<0.005, *** p<0.001, ns: no significant difference. Comparison between the two groups is analyzed by independent Sample's T-test. The ITC titration data and curves are reported in the Supporting Information (Tables S1–S4, Figures S15–S18).

The imprinting method works well for different proteins. Figure 4 shows that nanoparticles imprinted against horse radish peroxidase (HRP, M.W. ≈ 44 KDa, PI ≈ 7.2), β-galactosidase (β-Gal44, M.W. ≈ 430 KDa, PI ≈ 5.0), cytochrome C (cytc, M.W. ≈ 12 KDa, PI ≈ 12.4), and RNase A (M.W. ≈ 13.7 KDa, PI ≈ 8.6) all bind their templating proteins more strongly than nontemplating proteins. Thus, the method is applicable to both acidic and basic proteins, with the molecular weight spanning from 12 KDa all the way to 430 KDa.

Enzymes are biocatalysts for specific chemical reactions and their intracellular delivery can be used to correct enzymatic deficiencies or promote specific reactions within cells. Our initial enzyme to be delivered is HRP, whose activity can be measured by the catalytic oxidation of 3,3',5,5'-tetramethylbenzidine (TMB).[49] In these experiments, cells are first incubated with a 1:1 mixture of HRP and **NP**(HRP) for 12 h for facilitated uptake, followed by washing with PBS to remove any residual HRP and nanoparticles in the medium. After the cells are fixed with 4% formaldehyde, TMB and hydrogen peroxide are added. If HRPs have been delivered into the cells by the nanoparticles and remain active, TMB will be oxidized to form a dark green product. If no cell uptake has occurred during the incubation, a negative result will be obtained.

Figure 5 shows that the untreated cells (a) and the cells treated only with the substrate (b) display a negative result. The cells treated with HRP in the initial incubation and TMB after fixation (c) also fail to give any oxidation, indicating the enzyme is not taken up by the cells and is removed during the PBS washing step. On the other hand, when cells are incubated with both HRP and **NP**(HRP), washing does not remove the internalized enzyme, which oxidizes TMB after fixation and gives a positive result (d–e). As another control, the NINP control fails to give any oxidation (f), indicating that the molecular recognition of **NP**(HRP) is key to its intracellular delivery of HRP.

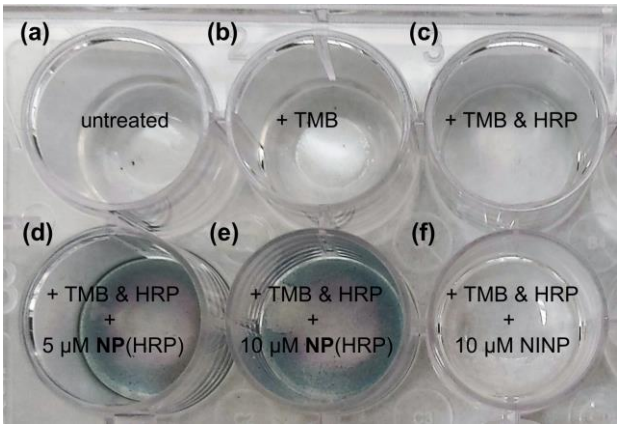

Figure 5. In cellulo HRP activity assay performed with MDA-MB-231 cells for the untreated sample (a), the sample only treated with TMB (b), the sample treated with TMB and HRP (c), the sample treated with TMB & HRP, plus 5 μM (d) or 10 μM (e) of **NP**(HRP), and the sample treated with TMB & HRP, plus 10 μM of NINP (f). [TMB] = 0.20 mM. [HRP] = 10 μM.

Our next enzyme to be delivered is β-Gal, which is able to hydrolyze *ortho*-nitrophenyl-β-galactoside (ONPG) to form yellow-colored *ortho*-nitrophenol that can be monitored by UV-vis

spectroscopy. Our initial experiments were performed in buffer and meant to help us understand whether binding with the nanoparticle compromises the catalytic activity of the enzyme (Figure 6a). The assay shows that NINPs at 100 μM have a negligible effect on the β-Gal activity. Binding with **NP**(β-Gal) does slow down the enzyme but the effect is modest. A hundred micromolar of the nanoparticle, for example, only reduces the enzyme activity by ~18%. Most of our cellular assay for β-Gal involves 20 μM of the nanoparticle. At this concentration, more than 95% of the enzyme activity is maintained according to Figure 6a.

Intracellular delivery of β-Gal by NP(β-Gal) into MDA-MB-231 cells was further validated by X-Gal staining. The experiments indicate that an intense blue-green staining of cells only occurs when the cells are treated with both β-Gal and **NP**(β-Gal), while the control samples give negligible staining (Figure S19).

Fluorescein di-β-D-galactopyranoside (FDG) is a substrate for β-Gal and its hydrolysis releases fluorescein, a green-emitting dye. Figure 6b shows the bright-field and fluorescent images of MDA-MB-231 cells treated under different conditions. All the cells are first incubated with β-Gal, plus other reagents as indicated at the bottom of the images. After 2 h, the cells are washed with PBS buffer to remove any residual β-Gal in the medium, followed by the addition of FDG. After further incubation for 6 h at 37 °C, the cells are imaged under a fluorescence microscope. Intense green fluorescence is only observed from those cells treated with β-Gal and **NP**(β-Gal), while the control samples give negligible fluorescence. These experiments demonstrate that our protein-binding nanoparticles not only can transport β-Gal into the cells, but the enzyme is also able to perform the desired reaction inside the cells.

Having established the successful intracellular delivery of catalytically active enzymes by our nanoparticles, we then turned our attention to two functional proteins and attempted to use the internalized proteins to modulate cellular functions.

Cytc is a protein located in the inner membrane of the mitochondrion and is involved in the respiratory electron transport chain (ETC).[50] When this protein is released from mitochondria, it triggers apoptosis by interacting with the apoptotic protease activating factor-1 (APAF1) to form apoptosome.[51,52] Thus, if active cyct is delivered into the cytosol, programmed cell death should occur.

Consistent with the above hypothesis, MTT assays indicate that, when MDA-MB-231cells are treated with an equimolar mixture of cytc and **NP**(cytc), a higher concentration of the mixture leads to increased cell death (Figure 7a). Control experiments reveal that nonimprinted nanoparticles (NINPs), **NP**(cytc) alone, or cytc alone all have minimal effects on the cell viability. Thus, although cytc triggers apoptosis, without the nanoparticle carrier, it cannot get inside cells and is nontoxic. Moreover, despite being cationic, **NP**(cytc) has low cytotoxicity toward cancer cells (Figure 7) or normal cells (Figure S25). Fluorescence-activated cell sorting (FACS) analysis of cytc-mediated apoptosis (Figure S20) also supports intracellular delivery of the protein by **NP**(cytc). In these experiments, the control sample treated with NINP + cytc consists of 98.4% live, 0.7% early apoptotic, 0.6% late apoptotic, and 0.3% dead cells. The sample treated with **NP**(cytc) + cytc consists of 6.7% live, 44.4% early apoptotic, 47.6% late apoptotic, and 1.4% dead cells.

Apoptosis is further studied by fluorescence microscopy. In these experiments, cells are first stained with acridine orange (AO, green in human cells) and ethidium bromide (EB, orange). AO stains both live and dead cells whereas EB only stains dead cells that have lost membrane integrity.[53] As a result, the double staining makes live cells appear uniformly green under a fluorescence microscope and those cells at early apoptosis appear as green dots in the nuclei. Cells at late apoptosis, whose membrane structures are compromised, appear orange. In agreement with the MTT assays, among the differently treated cells, only those with both cytc and **NP**(cytc) give an intense orange color in the red channel (Figure 8).

The above experiments indicate that protein molecules are delivered into the cytosol by the nanoparticles and then readily released to interact with cytosolic targets. This opens the possibility of delivering other proteins to manipulate cellular functions. RNase A, for example, cleaves single-stranded RNAs and has been investigated extensively to kill cancer cells.[54-58] To examine such a possibility, we

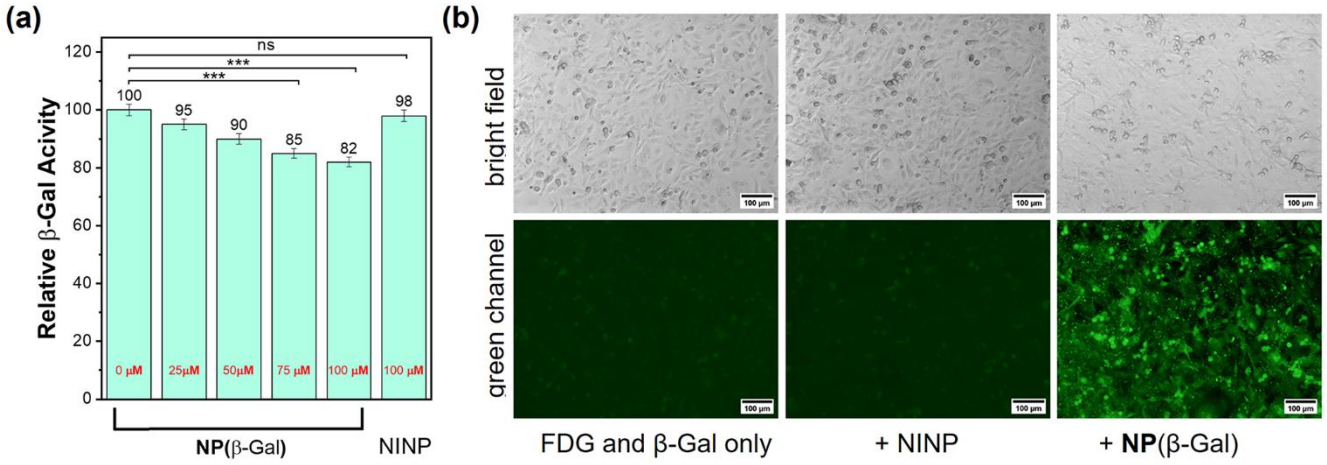

Figure 6. (**a**) Effects of **NP**(β-Gal) and NINP on β-Gal activity measured by the *ortho*-nitrophenyl-β-galactoside (ONPG) assay; Data are shown as mean ± SD. (n = 3). * $p<0.05$, ** $p<0.005$, *** $p<0.001$, ns: no significant difference. Comparison between the two groups is analyzed by independent Sample's T-test. (b) Fluorescence imaging of MDA-MB-231 cells for the *in cellulo* β-Gal activity. [β-Gal] = [**NP**(β-Gal)] = [NINP] = 20 μM**.** [FDG] = 10 μM.

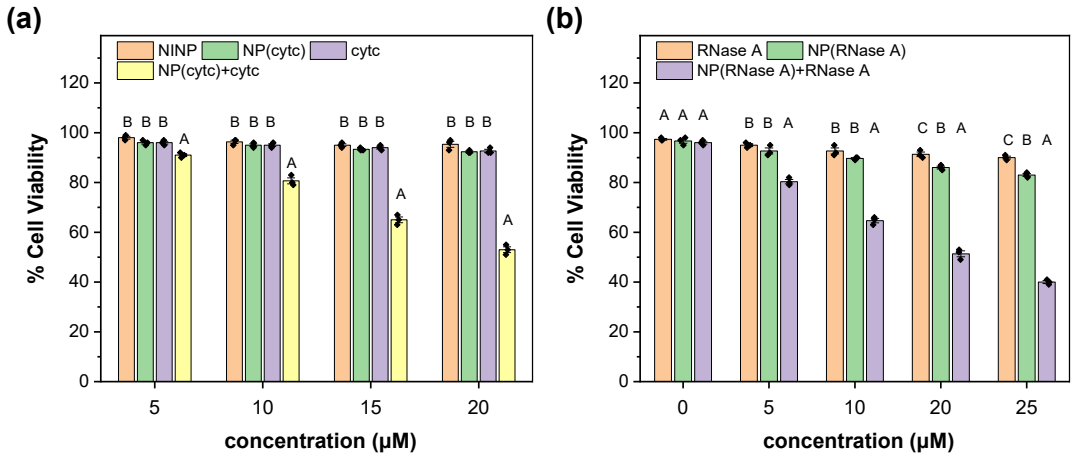

Figure 7. MTT assays of MDA-MB-231cells treated with (a) NINP, **NP**(cytc), cytc, and an equimolar mixture of **NP**(cytc) and cytc; and (b) RNase A, **NP**(RNase A), and an equimolar mixture of **NP**(RNase A) and RNase A. Treatments marked with the different letters are statistically significant ($P < 0.05$). Statistical analysis of the data is reported in the Supporting Information (Tables S5–S6, Figures S26–S27).

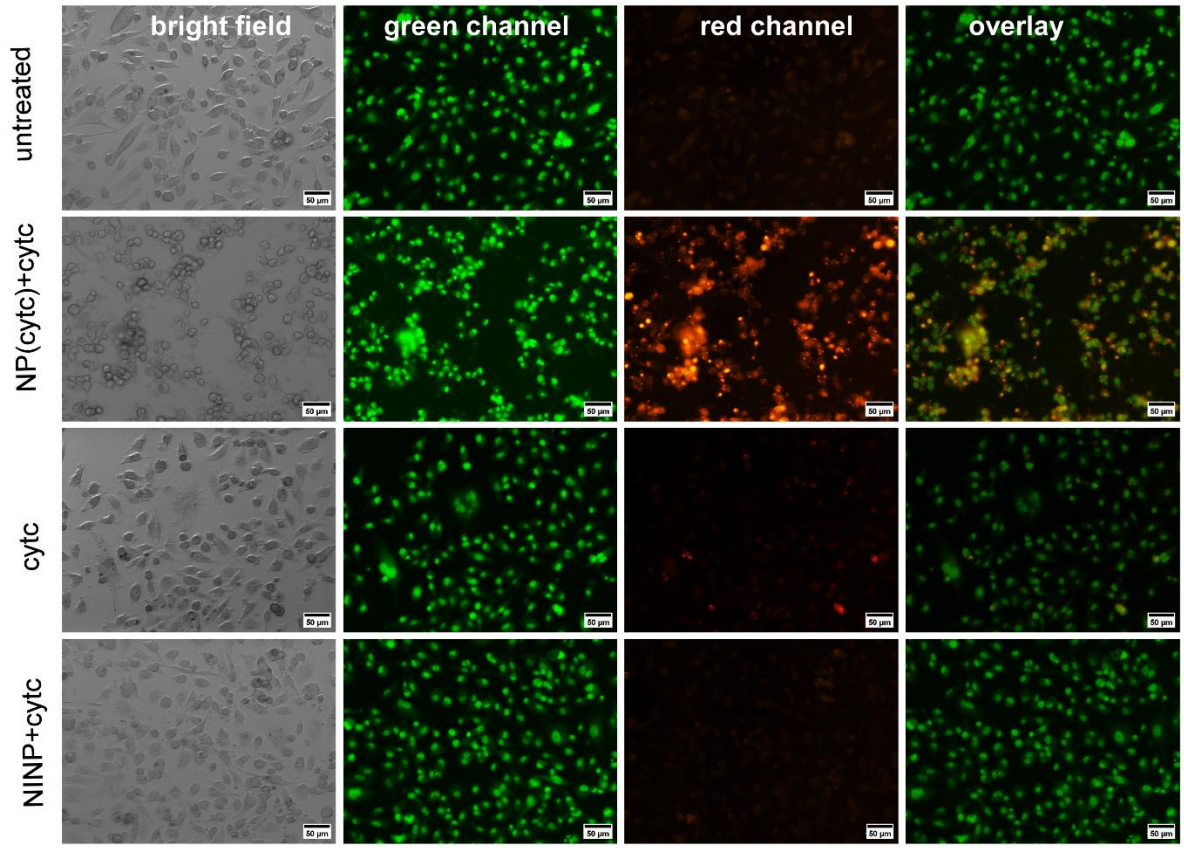

Figure 8. Images of AO/EB-stained MDA-MB-231cells treated with 20 μM of **NP**(cytc)+cytc, NINP+cytc, and cytc.

first stained MDA-MB-231cells with AO, which stains both DNAs and RNAs in live cells.[59] The dye molecules intercalated in DNAs show a green emission and those associated with RNAs (by electrostatic interactions) orange emission. Figure 9 shows that untreated cells give both green and orange emissions, indicating the presence of both DNAs and RNAs. The overlaid image shows largely yellow/green-colored cells. The cells treated with an equimolar mixture of RNase A and NINPs appear similarly. In contrast, the amounts of RNAs decrease dramatically for the cells treated with RNase A and **NP**(RNase A), consistent with cytosolic delivery of the enzyme and its ability to hydrolyze RNAs. In fact, the decrease of the orange emission is so severe that the overlaid image largely shows only a green color, indicating that most of RNAs in the cells have been hydrolyzed. Meanwhile, MTT assays indicate that up to 60% cell death has occurred in the samples treated with the RNase A and **NP**(RNase A) (Figure 7b). Neither control sample shows such behavior.

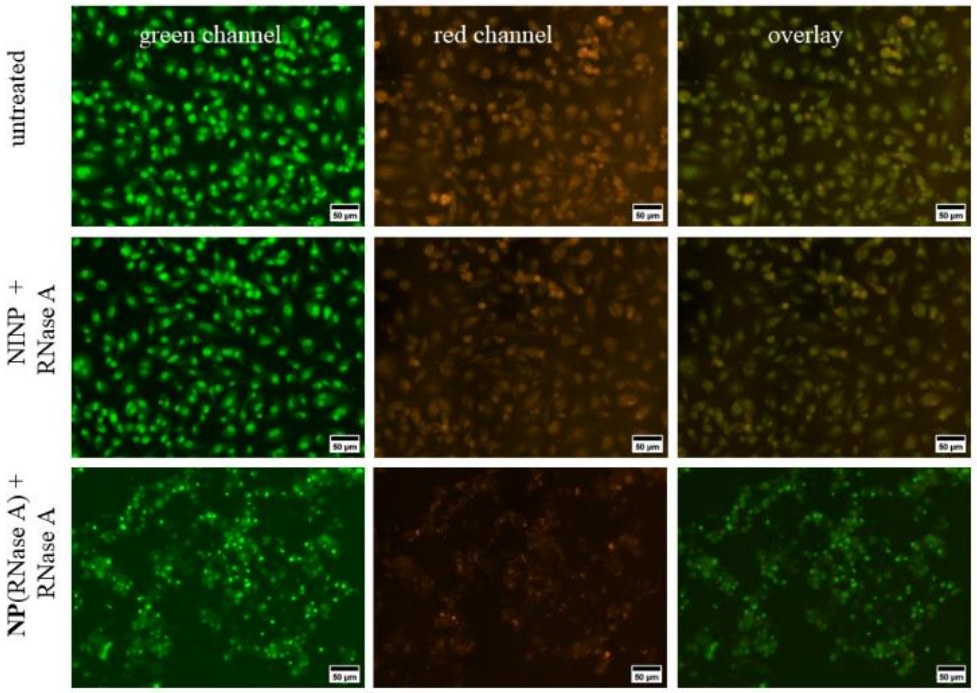

Figure 9. Fluorescent images of Acridine Orange (AO)-stained MDA-MB-231cells in apoptosis event induced by 20 μM NINP + 20 μM RNase A and 20 μM **NP**(RNase A) + 20 μM RNase A. Quantification of the fluorescence in the green channel is reported in Figure S21.

The RNase A-mediated RNA hydrolysis and cell death were additionally verified by propidium iodide (PI) imaging and FACS experiments. PI binds to DNA but cannot passively traverse plasma membranes. As a result, this dye accumulates only in dead cells whose plasma membranes become permeable whereas no uptake happens in live cells with intact membranes. Consistent with our results above, only the cells treated with both RNase A and **NP**(RNase A) are stained by PI (Figure S22–S24). More specifically, the control sample treated with NINP + RNase A consist of 96% live, 1% early apoptotic, 1% late apoptotic, and 2% dead cells. The sample treated with **NP**(RNase-A) + RNase-A consists of 5% live, 9% early apoptotic, 84% late apoptotic, and 2% dead cells.

CONCLUSIONS

Over 100 therapeutic proteins have been approved by the US FDA to treat various diseases and protein-based drugs frequently make it onto the list of the top-selling drugs.[3,4,60,61] Since most protein-delivery systems rely on endocytosis and escape of proteins from the endosomes is notoriously difficult, there is an urgent need to develop alternative strategies for protein delivery.[20,21]

In this work, we report a facile method for making water-soluble protein-binding nanoparticles from surfactant micelles. Direct imprinting of proteins has been very difficult to achieve but is made possible by the usage of trifluoromethyl ketone FMs that can interact with surface lysines of proteins in water quickly and reversibly. These ultrasmall nanoparticles bind their target proteins with high specificity. The micromolar binding affinities of the imprinted nanoparticles are strong enough for the protein cargo to be bound and transported into cells but weak enough for them to be released upon reaching the cytosol. They deliver proteins readily into the cytosol through a combination of energy-dependent and -independent pathways. The enzymes delivered into cells maintain their activity during the delivery and functional proteins may be introduced to regulate cellular functions such as induced apoptosis or RNA hydrolysis. The imprinting and the delivery work well for a range of proteins with varying molecular weights and isoelectric points. This type of doubly cross-linked nanoparticles have exceptional stability toward high temperatures,[62] organic solvents,[63] and strongly acidic conditions.[64] The nanoparticles can be readily functionalized with fluorescent labels, which allow their delivery and distribution to be monitored conveniently by fluorescence spectroscopy.

Methods and Materials

Materials. A typical procedure is as follows for the protein-binding nanoparticle preparation. To a micellar solution of compound **1** (9.3 mg, 0.02 mmol) in water (2.0 mL), N,N'-methylenebisacrylamide (MBAm, 0.04 mmol), compound **2** (0.008 mmol), and 2,2-dimethoxy-2-phenylacetophenone (DMPA, 10 μL of a 12.8 mg/mL solution in DMSO, 0.0005 mmol) were added. The mixture was subjected to ultrasonication for 10 min before compound **3** (3.4 mg, 0.02 mmol), $CuCl_2$ (10 μL of a 6.7 mg/mL solution in H_2O, 0.0005 mmol), and sodium ascorbate (10 μL of a 99 mg/mL solution in H_2O, 0.005 mmol) were added. After the reaction mixture was stirred slowly at room temperature for 12 h, F-BSA (0.0004 mmol) was added and the reaction mixture was stirred for 12 h. The reaction mixture was then transferred to a glass vial, purged with nitrogen for 15 min, sealed with a rubber septum, and irradiated in a Rayonet reactor for 12 h. Then, compound **4** (10.6 mg, 0.04 mmol), $CuCl_2$ (10 μL of a 6.7 mg/mL solution in H_2O, 0.0005 mmol), and sodium ascorbate (10 μL of a 99 mg/mL solution in H_2O, 0.005 mmol) were added, and the reaction mixture was stirred for another 6 h. The reaction mixture was poured into acetone (8 mL). The precipitate was collected by centrifugation and washed with a mixture of acetone/water (5 mL/1 mL) three times, methanol/acetic acid (5 mL/0.1 mL) three times, and then excess

methanol. The off-white powder was dried in air to afford the final **NP**(F-BSA) with a typical yield of ~80%.

For the **NP**(F-BSA)* preparation, after the irradiation in the Rayonet reactor for 12 h, compound **5** (0.001 mmol), $CuCl_2$ (20 μL of a 6.7 mg/mL solution in H_2O, 0.001 mmol), and sodium ascorbate (10 μL of a 99 mg/mL solution in H_2O, 0.01 mmol) was added to the mixture and stirred for 8 h in dark. Next, compound **4** (10.6 mg, 0.04 mmol), $CuCl_2$ (10 μL of a 6.7 mg/mL solution in H_2O, 0.0005 mmol), and sodium ascorbate (10 μL of a 99 mg/mL solution in H_2O, 0.005 mmol) were added, and the reaction mixture was stirred for another 6 h. The reaction mixture was poured into acetone (8 mL). The precipitate was collected by centrifugation and washed with a mixture of acetone/water (5 mL/1 mL) five times, methanol/acetic acid (5 mL/0.1 mL) three times, and then excess methanol. The light red powder was dried in air to afford the final **NP**(F-BSA)* with a typical yield of ~80%.

Cell Culture. The MDA-MB-231 cell line was acquired from ATCC. A-375 and SK-MEL-28 cells were received as a gift from Dr. Robbyn K Anand's lab at Iowa State University. MDA-MB-231 and A-375 cells were cultured in Dulbecco's Modified Eagle's Medium (DMEM) consisting of 100 mL/L of heat inactivated Fetal Bovine Serum (FBS) and 100 mg/L of antibiotics (penicillin, streptomycin and anti-fungal amphotericn B). SK-MEL28 cells were cultured in ATCC-formulated Eagle's Minimum Essential Medium (EMEM) consisting of 100 mL/L of heat inactivated Fetal Bovine Serum (FBS) and 100 mg/L of antibiotics (penicillin, streptomycin and anti-fungal amphotericn B). All the cell lines were maintained in a humid 5% CO_2 containing incubator until they reached 60–70% confluency. The cells were trypsinized (1× trypsin) and re-plated in fresh medium overnight prior to the experiments. The viable number of cells was determined using the Trypan blue exclusion test.

Cellular Uptake. Cellular uptake profile of F-BSA assisted by **NP**(F-BSA) was measured by capturing images in the green channel to monitor the FITC intensity. Briefly, the appropriate cells were incubated with 20 μM **NP**(F-BSA) + 20 μM F-BSA for 2 h. Then the cells were washed with PBS buffer 3 times before they were imaged under a fluorescence microscope. For confocal microscopy images, cells were seeded on a glass slide and fixed with 3.7% formaldehyde before imaging. Hoechst 33342 was used for staining the nuclei. Cells incubated with only F-BSA, NINP and PBS were used as negative controls.

The cellular internalization profile of **NP**(F-BSA)* was measured by lissamine rhodamine B-labelled **NP**(F-BSA). MDA-MB-231 and A-375 cells were incubated with 20 μM **NP**(F-BSA)* + 20 μM F-BSA for 2 h. The cells were washed with PBS buffer for 3 times before they were imaged under a fluorescence microscope in red channel.

Fluorescence-Activated Cell Sorting (FACS). The mean fluorescence intensity of **NP**(F-BSA)/F-BSA treated cells were evaluated by FACS experiment. Briefly, MDA-MB-231 cells were seeded onto 12-well plates and maintained in a humid 5% CO_2-containing incubator until they reached 60–70% confluency. The cells were treated with 5–20 μM **NP**(F-BSA)/F-BSA and incubated for 2 h. They were washed with cold phosphate-buffered saline (PBS) and harvested with 1 × trypsin. The washed cells were centrifugated and resuspended in the FACS-binding buffer to a density of ~1×10^6 cells/mL. The nanoparticle-stained cells were analyzed by flow cytometry in the green channel.

Cellular uptake Mechanism of NP(F-BSA). Cellular uptake mechanism of F-BSA/**NP**(F-BSA) was evaluated in the presence of different endocytosis inhibitors. Briefly, MDA-MB-231 cells were seeded onto 6-well plates, and incubated with 20 μM F-BSA and 20 μM **NP**(F-BSA) for 2 h after treatment with methyl-β-cyclodextrin (5.0 mM for 30 min), sucrose (0.45 M for 10 min), chlorpromazine (20 μg/mL for 45 min), amiloride (1 mM for 30 min), and sodium azide/2-deoxy-D-glucose (10 & 6 mM, respectively, for 1 h). The mean fluorescence intensity (MFI) was measured using the BD-FACS Area III flow cytometer.

DIC Imaging in-cellulo β-Gal Activity. Intracellular delivery of β-Gal by **NP**(β-Gal) into MDA-MB-231 cells was determined by X-Gal staining. Briefly, the cells were treated with 20 μM **NP**(β-Gal) and 20 μM β-Gal, followed by incubation for 12 h at 37°C. Then the cells were washed with PBS and fixed with 3.7 % formaldehyde for 10 min at room temperature. Next, the cells were incubated with the working solution of X-Gal (containing 50 μg/mL of X-Gal) of overnight at 37 °C. The cells were washed and bright field images of the cells were captured under an inverted microscope.

Fluorescence Imaging β-Gal Activity. Intracellular delivery of β-Gal by **NP**(β-Gal) into MDA-MB-231 cells was measured by fluorogenic substrate fluorescein di(β-D galactopyranoside) (FDG). Briefly, the cells were treated with 20 μM **NP**(β-Gal) and 20 μM β-Gal, followed by incubation for 12 h at 37 °C. Then the cells were incubated with the 50 μM of fluorescein di(β-D galactopyranoside) at 37 °C for 6 h. Finally, the cells were washed and the images of the cells were captured under fluorescence microscope in green channel.

Cytotoxicity Assay. The viable cells after treatment were analyzed using the 3(4,5-dimethylthiazolyl-2)2,5-diphenyltetrazolium bromide assay (MTT, Sigma-Aldrich) according to the manufacturer's protocol. The cells were seeded onto 96 well plates overnight, followed by treatment with different concentrations of **NP**(RNase-A) + RNase-A or **NP**(cytc) + cytc, respectively for 12 h. Control experiments were carried out with **NINP**, **NP**(RNase-A), or **NP**(cytc). After incubation, the previous medium was removed and the cells were reconstituted with colorless DMEM, followed by the addition of MTT solution to a final concentration of 0.5 mg/mL in each well. Then, the cells containing MTT were incubated for 4 h at 37 °C. The media was removed again carefully, followed by the addition of 100 μL DMSO to each well. Then the plates were rocked gently for 10 min to ensure proper mixing. Finally, the absorbance at 570 and 575 nm was measured using a micro plate reader. Cell viability was defined as the percentage of live cells relative to the untreated controls.

AO/EtBr Staining. The cellular apoptosis event after treatment with **NP**(cytc) + cytc were evaluated by AO/ EtBr staining. Briefly, MDA-MB-231 cells were seeded onto 12-well plates and incubated at 37 °C for 24 h to reach a cellular density of approx. 5×10^5 cells per well, followed by treatment with 20 μM **NP**(cytc) and 20 μM cytc. The cells were incubated for 12 h and then washed with PBS, trypsinized and resuspended in fresh 20 μL of fresh PBS. A 5.0 μL aliquot of a mixture of 100 μg/mL AO and 100 μg/mL EB solutions was added to the cells and the cells were incubated in dark for 5 min. Then a 10 μL suspension of cells was spread onto a microscope slide and covered with a glass coverslip. At least 400 cells were examined under a fluorescence microscope.

AO Staining for RNase-A-mediated RNA Degradation.

NP(RNase-A)/RNase-A mediated RNA degradation and consequent apoptosis in MDA-MB-231 cells was evaluated by AO staining experiment. Briefly, MDA-MB-231 cells were seeded onto 12-well plates and incubated at 37 °C for 24 h to reach a cellular density of approx. 5 $\times 10^5$ cells per well, followed by treatment with 20 μM **NP**(RNase-A) and 20 μM RNase-A. The cells were then incubated for 6 h. Next, the cells were washed, trypsinized, and resuspended in PBS. A 5.0 μL aliquot of a 100 μg/mL AO solution was added to the cells and incubated in dark for 5 min. Then a 10 μL suspension of cells was spread onto a microscope slide and covered with a glass coverslip. At least 400 cells were examined under a fluorescence microscope. AO produces orange fluorescence when it binds to RNA and green fluorescence when it binds to DNA. The enhanced intensity in both the green and red channels with respect to untreated control were recorded to establish the RNA degradation and apoptosis.

PI staining for RNase-A Mediated Apoptosis. NP(RNase-A) + RNase-A mediated RNA degradation and consequent apoptotic cell death in MDA-MB-231 cells were further confirmed by PI imaging. Briefly, MDA-MB-231 and A-375 cells were seeded onto 12-well plates and incubated at 37 °C for 24 h to reach a cellular density of approx. 5 $\times 10^5$ cells per well, followed by treatment with 20 μM **NP**(RNase-A) and 20 μM RNase-A. After incubation for 6 h, the cells were washed, trypsinized and resuspended in PBS. A PI (1mg/mL) solution was added to the cell suspension to reach final concentration of 2 μg/ml and incubated in dark for 15 min. Then a 10 μL suspension of cells was spread onto a microscope slide and covered with a glass coverslip. At least 400 cells were examined under a fluorescence microscope in red channel (only the dead cells were stained by PI in red channel)

Apoptosis Measurement with Annexin V/PI in Flow Cytometry. The percentage of dead cells were measured using apoptosis kits with annexin V conjugates including Alexa Fluor 488 and PI (Thermo fisher, Catalog number: V13241) following the manufacturer's protocol. Briefly, MDA-MB-231 cells were seeded onto 6-well plates, followed by treatment with 20 μM of **NP**(cyt-c) + cyt-c or **NP**(RNAse-A) + RNAse-A for 12 h. The cells were then washed with a cold phosphate-buffered saline (PBS) and harvested with 1× trypsin. The cells were centrifugated and resuspended in 1× annexin-binding buffer to a density of ~1×10^6 cells/mL. Then, 5 μL of Alexa Fluor 488 Annexin V (supplied with kit) and 1 μL of the 100 μg/mL PI working solution was added to each 100 μL of cell suspension. The cells were incubated at room temperature for 15 min in dark, followed by the addition of 400 μL of 1× annexin-binding buffer. After gentle mixing, the cells were kept on ice before they were analyzed by flow cytometry.

ASSOCIATED CONTENT

Supporting Information

Synthetic procedures for small molecules, characterization of compounds and materials, ITC binding curves, additional tables and figures, NMR data, and statistical analysis of the data. This material is available free of charge via the Internet at http://pubs.acs.org.

AUTHOR INFORMATION

Corresponding Author

Yan Zhao – Department of Chemistry, Iowa State University, Ames, Iowa 50011-3111, U.S.A.; E-mail: zhaoy@iastate.edu

Authors

Avijit Ghosh – Department of Chemistry, Iowa State University, Ames, Iowa 50011-3111, U.S.A.
Mansi Sharma – Department of Chemistry, Iowa State University, Ames, Iowa 50011-3111, U.S.A.

ORCID

Avijit Ghosh: 0000-0002-8974-9565
Mansi Sharma: 0009-0003-4728-9972
Yan Zhao: 0000-0003-1215-2565

ACKNOWLEDGMENT

We thank NSF (DMR-2308625) for supporting the research.

REFERENCES

(1) Chen, N.; He, Y.; Zang, M.; Zhang, Y.; Lu, H.; Zhao, Q.; Wang, S.; Gao, Y. Approaches and materials for endocytosis-independent intracellular delivery of proteins. *Biomaterials* **2022**, *286*, 121567.
(2) Chan, A.; Tsourkas, A. Intracellular Protein Delivery: Approaches, Challenges, and Clinical Applications. *BME Front.* **2024**, *5*, 0035.
(3) Lu, R. M.; Hwang, Y. C.; Liu, I. J.; Lee, C. C.; Tsai, H. Z.; Li, H. J.; Wu, H. C. Development of therapeutic antibodies for the treatment of diseases. *J. Biomed. Sci.* **2020**, *27*, 1.
(4) Brown, A. Top product forecasts for 2023. *Nat. Rev. Drug Discov.* **2023**, *22*, 8.
(5) Heitz, F.; Morris, M. C.; Divita, G. Twenty years of cell-penetrating peptides: from molecular mechanisms to therapeutics. *Br. J. Pharmacol.* **2009**, *157*, 195-206.
(6) Lundberg, M.; Johansson, M. Is VP22 nuclear homing an artifact? *Nat. Biotechnol.* **2001**, *19*, 713-713.
(7) Dutta, K.; Hu, D.; Zhao, B.; Ribbe, A. E.; Zhuang, J.; Thayumanavan, S. Templated Self-Assembly of a Covalent Polymer Network for Intracellular Protein Delivery and Traceless Release. *J. Am. Chem. Soc.* **2017**, *139*, 5676-5679.
(8) Liu, C. Y.; Wan, T.; Wang, H.; Zhang, S.; Ping, Y.; Cheng, Y. Y. A boronic acid-rich dendrimer with robust and unprecedented efficiency for cytosolic protein delivery and CRISPR-Cas9 gene editing. *Sci. Adv.* **2019**, *5*, eaaw8922.
(9) Kretzmann, J. A.; Luther, D. C.; Evans, C. W.; Jeon, T.; Jerome, W.; Gopalakrishnan, S.; Lee, Y. W.; Norret, M.; Iyer, K. S.; Rotello, V. M. Regulation of Proteins to the Cytosol Using Delivery Systems with Engineered Polymer Architecture. *J. Am. Chem. Soc.* **2021**, *143*, 4758-4765.
(10) Yin, J.; Wang, Q.; Hou, S.; Bao, L.; Yao, W.; Gao, X. Potent Protein Delivery into Mammalian Cells via a Supercharged Polypeptide. *J. Am. Chem. Soc.* **2018**, *140*, 17234-17240.
(11) Yang, Y.; Zhu, H.; Liu, D.; Luo, H.; Chang, R.; Ji, Y.; Yao, W.; Yin, J.; Gao, X. A Versatile Platform for the Tumor-Targeted Intracellular Delivery of Peptides, Proteins, and siRNA. *Adv. Funct. Mater.* **2023**, *33*, 2301011.
(12) Yu, S.; Yang, H.; Li, T.; Pan, H.; Ren, S.; Luo, G.; Jiang, J.; Yu, L.; Chen, B.; Zhang, Y.; Wang, S.; Tian, R.; Zhang, T.; Zhang, S.; Chen, Y.; Yuan, Q.; Ge, S.; Zhang, J.; Xia, N. Efficient intracellular delivery of proteins by a multifunctional chimaeric peptide in vitro and in vivo. *Nat. Commun.* **2021**, *12*, 5131.
(13) Roh, H.; Dorner, B. G.; Ting, A. Y. Cell-Type-Specific Intracellular Protein Delivery with Inactivated Botulinum Neurotoxin. *J. Am. Chem. Soc.* **2023**, *145*, 10220-10226.
(14) Sugiman-Marangos, S. N.; Beilhartz, G. L.; Zhao, X.; Zhou, D.; Hua, R.; Kim, P. K.; Rini, J. M.; Minassian, B. A.; Melnyk, R. A. Exploiting the diphtheria toxin internalization receptor enhances delivery of proteins to lysosomes for enzyme replacement therapy. *Sci. Adv.* **2020**, *6*, eabb0385.
(15) Banskota, S.; Raguram, A.; Suh, S.; Du, S. W.; Davis, J. R.; Choi, E. H.; Wang, X.; Nielsen, S. C.; Newby, G. A.; Randolph, P. B.; Osborn, M. J.; Musunuru, K.; Palczewski, K.; Liu, D. R. Engineered virus-like particles for efficient in vivo delivery of therapeutic proteins. *Cell* **2022**, *185*, 250-265.e216.
(16) Kreitz, J.; Friedrich, M. J.; Guru, A.; Lash, B.; Saito, M.; Macrae, R. K.; Zhang, F. Programmable protein delivery with a bacterial contractile injection system. *Nature* **2023**, *616*, 357-364.

(17) D'Astolfo, D. S.; Pagliero, R. J.; Pras, A.; Karthaus, W. R.; Clevers, H.; Prasad, V.; Lebbink, R. J.; Rehmann, H.; Geijsen, N. Efficient intracellular delivery of native proteins. *Cell* **2015**, *161*, 674-690.
(18) van Dun, S.; Ottmann, C.; Milroy, L.-G.; Brunsveld, L. Supramolecular Chemistry Targeting Proteins. *J. Am. Chem. Soc.* **2017**, *139*, 13960-13968.
(19) Mabonga, L.; Kappo, A. P. Protein-protein interaction modulators: advances, successes and remaining challenges. *Biophys. Rev.* **2019**, *11*, 559-581.
(20) Canton, I.; Battaglia, G. Endocytosis at the nanoscale. *Chem. Soc. Rev.* **2012**, *41*, 2718-2739.
(21) Selby, L. I.; Cortez‐Jugo, C. M.; Such, G. K.; Johnston, A. P. Nanoescapology: progress toward understanding the endosomal escape of polymeric nanoparticles. *Wiley Interdiscip. Rev. Nanomed. Nanobiotechnol.* **2017**, *9*, e1452.
(22) Pan, J.; Chen, W.; Ma, Y.; Pan, G. Molecularly imprinted polymers as receptor mimics for selective cell recognition. *Chem. Soc. Rev.* **2018**, *47*, 5574-5587.
(23) Zhang, H. Molecularly Imprinted Nanoparticles for Biomedical Applications. *Adv. Mater.* **2020**, *32*, 1806328.
(24) Haupt, K.; Medina Rangel, P. X.; Bui, B. T. S. Molecularly Imprinted Polymers: Antibody Mimics for Bioimaging and Therapy. *Chem. Rev.* **2020**, *120*, 9554-9582.
(25) He, Y.; Lin, Z. Recent advances in protein-imprinted polymers: synthesis, applications and challenges. *J. Mater. Chem. B* **2022**, *10*, 6571-6589.
(26) Chen, K.; Zhao, Y. Molecular recognition of enzymes and modulation of enzymatic activity by nanoparticle conformational sensors. *Chem. Commun.* **2022**, *58*, 1732-1735.
(27) Panja, P.; Jana, N. R. Arginine-Terminated Nanoparticles of <10 nm Size for Direct Membrane Penetration and Protein Delivery for Straight Access to Cytosol and Nucleus. *J. Phys. Chem. Lett.* **2020**, *11*, 2363-2368.
(28) Li, X.; Zhao, Y. Protection/Deprotection of Surface Activity and Its Applications in the Controlled Release of Liposomal Contents. *Langmuir* **2012**, *28*, 4152-4159.
(29) Mohr, G. J.; Demuth, C.; Spichiger-Keller, U. E. Application of chromogenic and fluorogenic reactands in the optical sensing of dissolved aliphatic amines. *Anal. Chem.* **1998**, *70*, 3868-3873.
(30) Mohr, G. J.; Citterio, D.; Demuth, C.; Fehlmann, M.; Jenny, L.; Lohse, C.; Moradian, A.; Nezel, T.; Rothmaier, M.; Spichiger, U. E. Reversible chemical reactions as the basis for optical sensors used to detect amines, alcohols and humidity. *J. Mater. Chem.* **1999**, *9*, 2259-2264.
(31) Ryu, D.; Park, E.; Kim, D.-S.; Yan, S.; Lee, J. Y.; Chang, B.-Y.; Ahn, K. H. A Rational Approach to Fluorescence "Turn-On" Sensing of α-Amino-carboxylates. *J. Am. Chem. Soc.* **2008**, *130*, 2394-2395.
(32) Rowan, S. J.; Cantrill, S. J.; Cousins, G. R.; Sanders, J. K.; Stoddart, J. F. Dynamic covalent chemistry. *Angew. Chem. Int. Ed.* **2002**, *41*, 898-952.
(33) Jin, Y.; Yu, C.; Denman, R. J.; Zhang, W. Recent advances in dynamic covalent chemistry. *Chem. Soc. Rev.* **2013**, *42*, 6634-6654.
(34) Zou, W.; Dong, J.; Luo, Y.; Zhao, Q.; Xie, T. Dynamic covalent polymer networks: from old chemistry to modern day innovations. *Adv. Mater.* **2017**, *29*, 1606100.
(35) Chakma, P.; Konkolewicz, D. Dynamic Covalent Bonds in Polymeric Materials. *Angew. Chem. Int. Ed.* **2019**, *58*, 9682-9695.
(36) Zangiabadi, M.; Zhao, Y. Selective Binding of Complex Glycans and Glycoproteins in Water by Molecularly Imprinted Nanoparticles. *Nano Lett.* **2020**, *20*, 5106-5110.
(37) Fa, S.; Zhao, Y. General Method for Peptide Recognition in Water through Bioinspired Complementarity. *Chem. Mater.* **2019**, *31*, 4889-4896.
(38) Miller, C. R.; Bondurant, B.; McLean, S. D.; McGovern, K. A.; O'Brien, D. F. Liposome−Cell Interactions in Vitro: Effect of Liposome Surface Charge on the Binding and Endocytosis of Conventional and Sterically Stabilized Liposomes. *Biochemistry* **1998**, *37*, 12875-12883.
(39) Cho, E. C.; Xie, J.; Wurm, P. A.; Xia, Y. Understanding the Role of Surface Charges in Cellular Adsorption versus Internalization by Selectively Removing Gold Nanoparticles on the Cell Surface with a I2/KI Etchant. *Nano Lett.* **2009**, *9*, 1080-1084.
(40) Asati, A.; Santra, S.; Kaittanis, C.; Perez, J. M. Surface-Charge-Dependent Cell Localization and Cytotoxicity of Cerium Oxide Nanoparticles. *ACS Nano* **2010**, *4*, 5321-5331.
(41) Jiang, Y.; Huo, S.; Mizuhara, T.; Das, R.; Lee, Y. W.; Hou, S.; Moyano, D. F.; Duncan, B.; Liang, X. J.; Rotello, V. M. The Interplay of Size and Surface Functionality on the Cellular Uptake of Sub-10 nm Gold Nanoparticles. *ACS Nano* **2015**, *9*, 9986-9993.
(42) Rennick, J. J.; Johnston, A. P. R.; Parton, R. G. Key principles and methods for studying the endocytosis of biological and nanoparticle therapeutics. *Nat. Nanotechnol.* **2021**, *16*, 266-276.
(43) Debnath, K.; Pal, S.; Jana, N. R. Chemically Designed Nanoscale Materials for Controlling Cellular Processes. *Acc. Chem. Res.* **2021**, *54*, 2916-2927.
(44) Sousa de Almeida, M.; Susnik, E.; Drasler, B.; Taladriz-Blanco, P.; Petri-Fink, A.; Rothen-Rutishauser, B. Understanding nanoparticle endocytosis to improve targeting strategies in nanomedicine. *Chem. Soc. Rev.* **2021**, *50*, 5397-5434.
(45) Koivusalo, M.; Welch, C.; Hayashi, H.; Scott, C. C.; Kim, M.; Alexander, T.; Touret, N.; Hahn, K. M.; Grinstein, S. Amiloride inhibits macropinocytosis by lowering submembranous pH and preventing Rac1 and Cdc42 signaling. *J. Cell Biol.* **2010**, *188*, 547-563.
(46) Rodal, S. K.; Skretting, G.; Garred, Ø.; Vilhardt, F.; Deurs, B. v.; Sandvig, K. Extraction of Cholesterol with Methyl-β-Cyclodextrin Perturbs Formation of Clathrin-coated Endocytic Vesicles. *Mol. Biol. Cell* **1999**, *10*, 961-974.
(47) Nabi, I. R.; Le, P. U. Caveolae/raft-dependent endocytosis. *J. Cell Biol.* **2003**, *161*, 673-677.
(48) Timney, B. L.; Raveh, B.; Mironska, R.; Trivedi, J. M.; Kim, S. J.; Russel, D.; Wente, S. R.; Sali, A.; Rout, M. P. Simple rules for passive diffusion through the nuclear pore complex. *J. Cell Biol.* **2016**, *215*, 57-76.
(49) Bos, E.; Van der Doelen, A.; Rooy, N. v.; Schuurs, A. H. 3, 3′, 5, 5′-Tetramethylbenzidine as an Ames test negative chromogen for horse-radish peroxidase in enzyme-immunoassay. *J. Immunoass. Immunochem.* **1981**, *2*, 187-204.
(50) Ferguson-Miller, S.; Brautigan, D.; Margoliash, E. Definition of cytochrome c binding domains by chemical modification. III. Kinetics of reaction of carboxydinitrophenyl cytochromes c with cytochrome c oxidase. *J. Biol. Chem* **1978**, *253*, 149-159.
(51) Jiang, X.; Wang, X. Cytochrome C-mediated apoptosis. *Annu. Rev. Biochem.* **2004**, *73*, 87-106.
(52) Ow, Y.-L. P.; Green, D. R.; Hao, Z.; Mak, T. W. Cytochrome c: functions beyond respiration. *Nat. Rev. Mol. Cell Biol.* **2008**, *9*, 532-542.
(53) Kasibhatla, S.; Amarante-Mendes, G. P.; Finucane, D.; Brunner, T.; Bossy-Wetzel, E.; Green, D. R. Acridine Orange/Ethidium Bromide (AO/EB) Staining to Detect Apoptosis. *Cold Spring Harb. Protoc.* **2006**, *2006*, pdb.prot4493.
(54) Leland, P. A.; Staniszewski, K. E.; Kim, B. M.; Raines, R. T. Endowing human pancreatic ribonuclease with toxicity for cancer cells. *J. Biol. Chem.* **2001**, *276*, 43095-43102.
(55) Krauss, J.; Arndt, M. A.; Dubel, S.; Rybak, S. M. Antibody-targeted RNase fusion proteins (immunoRNases) for cancer therapy. *Curr. Pharm. Biotechnol.* **2008**, *9*, 231-234.
(56) Liu, X.; Zhang, P.; He, D.; Rödl, W.; Preiß, T.; Rädler, J. O.; Wagner, E.; Lächelt, U. pH-reversible cationic RNase A conjugates for enhanced cellular delivery and tumor cell killing. *Biomacromolecules* **2016**, *17*, 173-182.
(57) Zhao, S.; Duan, F.; Liu, S.; Wu, T.; Shang, Y.; Tian, R.; Liu, J.; Wang, Z.-G.; Jiang, Q.; Ding, B. Efficient intracellular delivery of RNase A using DNA origami carriers. *ACS Appl Mater Interfaces* **2019**, *11*, 11112-11118.
(58) Zhao, Y.; Jia, R.; Liu, Y.; Shen, X.; Wang, H.; Yuan, L. Specific photothermal killing of cancer cells by RNase-conjugated glyco-gold nanoparticles. *Mater. Today Commun.* **2021**, *28*, 102640.
(59) Darzynkiewicz, Z. In *Methods Cell Biol.*; Darzynkiewicz, Z., Crissman, H. A., Eds.; Academic Press, 1990; Vol. 33; pp 285-298.
(60) Leader, B.; Baca, Q. J.; Golan, D. E. Protein therapeutics: a summary and pharmacological classification. *Nat. Rev. Drug Discov.* **2008**, *7*, 21-39.
(61) Dimitrov, D. S. Therapeutic proteins. *Methods Mol. Biol.* **2012**, *899*, 1-26.
(62) Zangiabadi, M.; Zhao, Y. Synergistic Hydrolysis of Cellulose by a Blend of Cellulase-Mimicking Polymeric Nanoparticle Catalysts. *J. Am. Chem. Soc.* **2022**, *144*, 17110-17119.
(63) Li, X.; Zangiabadi, M.; Zhao, Y. Molecularly Imprinted Synthetic Glucosidase for the Hydrolysis of Cellulose in Aqueous and Nonaqueous Solutions. *J. Am. Chem. Soc.* **2021**, *143*, 5172-5181.
(64) Xing, X.; Zhao, Y. Fluorescent nanoparticle sensors with tailor-made recognition units and proximate fluorescent reporter groups. *New J. Chem.* **2018**, *42*, 9377-9380.